J Mater Sci: Mater Electron (2016) 27:6835–6844
DOI 10.1007/s10854-016-4635-x

CrossMark

Comparative study of the microstructure and mechanical strength of tin-copper (Sn0.7Cu) solder modified with silver (Ag) by both alloying and doping methods

Ze Zhu[1] · Huayu Sun[1] · Fengshun Wu[2] · Yan-cheong Chan[1]

Received: 19 December 2015 / Accepted: 4 March 2016 / Published online: 9 March 2016
© Springer Science+Business Media New York 2016

Abstract In order to compare the effectiveness of alloying methods with doping methods, we have studied the microstructure and mechanical strength of Sn0.7Cu solder and two kinds of Ag modified Sn0.7Cu solders, i.e., Sn0.7Cu0.3Ag (prepared by alloying pure Sn, Cu, and Ag metals) and Sn0.7Cu + 0.3Ag (prepared by doping Ag nanoparticles into Sn0.7Cu). Solder joints were sent for mechanical tests and microstructure observation after aging at 90 °C for up to 500 h. Electromigration (EM) test models were built to evaluate the resistance of solders to EM degradation at an average current density of 0.79×10^4 A/cm^2. Experimental results revealed that both Ag modified Sn0.7Cu solders had higher mechanical strength and stronger resistance to EM than Sn0.7Cu. This improvement was due to the introduction of dispersed Ag_3Sn intermetallic compounds (IMCs), which acted as a second phase to refine the bulk solder, stop dislocations and hinder atomic migration. Sn0.7Cu0.3Ag was found to be more effective in reinforcing the mechanical strength than Sn0.7Cu + 0.3Ag, since the shear strength and microhardness of the former solder were respectively 12.79 % and 1.01 % higher than the latter one. The products of diffusivity and effective charge number DZ^*, which represented the EM rate, for Cu atoms were measured to be 3.49×10^{-9}, 1.91×10^{-9}, 2.64×10^{-9} cm^2/s for Sn0.7Cu, Sn0.7Cu0.3Ag, and Sn0.7Cu + 0.3Ag, respectively. The superior performance of Sn0.7Cu0.3Ag was ascribed to the smaller size and wider distribution of Ag_3Sn IMCs in the solder matrix. To conclude, the alloying method produced greater improvement than the doping method in the microstructure and mechanical strength of Sn0.7Cu solder.

✉ Ze Zhu
peterchu93@gmail.com; zezhu2-c@cityu.edu.hk

[1] Department of Electronics Engineering, City University of Hong Kong, Room 2386, Fong Yun-wah Building, Kowloon Tong, Hong Kong, S.A.R., People's Republic of China

[2] Institute of Material Science and Engineering, Huazhong University of Science and Technology, Wuhan, People's Republic of China

1 Introduction

Lead (Pb) free solders have been studied for replacement of the toxic Pb containing solders in recent decades, due to the 'Directive of the Restriction of the Use of Certain Hazardous Substances' (RoHS) [1, 2]. Various lead-free solders have been proposed. For example, tin–silver–copper (Sn–Ag–Cu), tin–silver (Sn–Ag), tin–copper (Sn–Cu), and tin–bismuth (Sn-Bi) based solders [2]. Sn–Ag–Cu solders, especially Sn3.0Ag0.5Cu, were recognized as the best candidates for replacement of traditional Sn37Pb solder, because of their superior mechanical strength and good solderability [2, 3]. However, the high silver content increases the cost of the solder, since current prices are 14.91 USD/OZT (218.17 USD/LB) for Ag, 7.10 USD/LB for Sn, and 2.40 USD/LB for Cu [4]. The electronics industry demands low cost solder to reduce the manufacturing cost [5]. Sn0.7Cu and Sn0.7Cu0.3Ag solders have attracted a lot of interests due to their low cost.

There are two approaches [6] to add metallic elements into solders: (1) alloying [7], where pure metals are melted, mixed, sintered, and cooled to form solder paste—and (2) doping [8], where metallic nanoparticles are doped into solder paste. Nanodoping has proved to be effective in refining microstructure, inhibiting excessive growth of interfacial intermetallic compounds (IMCs), and reinforcing

the mechanical strength of solder joints [9–13]. Li et al. [14] have studied the effect of Ag nanoparticles on the microstructure and mechanical properties of Sn58Bi. The interfacial IMC growth rate was lowered by 39.7 % in 1 wt % Ag nanoparticle-doped Sn58Bi-Ag solder. The mechanical strength was also enhanced, since the hardness was increased by 12.2 % and the shear strength was reinforced by 18.9 %. Bashir et al. [15] have investigated the impact of Ni nanoparticles on Sn3.0Ag0.5Cu solder. The experimental results revealed that the IMC layer growth at both anodes and cathodes was inhibited and the polarity effect due to current stressing was suppressed when 2 wt % of Ni nanoparticles was added. Similar results were also reported by other researchers [10, 16–18]. The effect of the alloying method was investigated by Chen et al. [5], who found that, by adding 0.1 wt % Cr, the microstructure of Sn-9Zn solder was refined and the oxidation at the subsurface was prevented.

All these papers compared the performance of pristine solder and modified solder. However, only a few investigations have been carried out to compare the relative effectiveness of the alloying method and the doping method. Since alloying and doping methods incorporate metals in different morphologies and undergo different processes, the chances are that the microstructures, as well as the mechanical strength, are different in the two solders. In this paper, we have investigated the effects of Ag addition on Sn0.7Cu solder for two different methods. Sn0.7Cu0.3Ag was made by the alloying method, and Sn0.7Cu + 0.3Ag was made by doping 0.3 wt % Ag nanoparticles into Sn0.7Cu solder paste. These two solder pastes were identical in elemental composition, which helps to focus on the differences arising from the adding method. Solder joints and interconnects were subjected to a series of experiments—such as shear strength testing, hardness testing and also current stress testing—in order to characterize their mechanical strength and microstructure evolution.

2 Experiments

Sn0.7Cu solder paste (Purity 85.7 %, from Amtech.) and Sn0.7Cu0.3Ag solder paste (Purity 85.7 %, from Amtech.) were prepared by alloying pure metals. The composite Sn0.7Cu + 0.3Ag solder was prepared by doping Ag nanoparticles (Purity 99.9 %, diameter 70 nm, from Hongwu Tech.) into Sn0.7Cu solder paste, followed by stirring for 1 h to achieve a uniform distribution. The amount of Ag nanoparticles was 0.3 wt % of Sn0.7Cu, with solder flux deducted according to the purity. The elemental compositions of the three solders are listed in Table 1. The three types of solder were then printed on a glazed ceramic substrate through a stencil (of thickness 0.15 mm), followed by reflowing in an eight-zone convection reflow oven (BTU Pyramax-100 N) to fabricate solder balls according to a reflow profile with a peak temperature of 260 °C (533 K) and a reflow zone of 80 s. After ultrasonic cleaning and drying, the solder balls were screened to a maximum diameter of 380 μm. Differential Scanning Calorimetry (DSC, Universal V2.6D TA Instruments) was used to study the heat flow of three solders with 14 mg samples sealed in a hermetic aluminum pan. The scanning temperature range was from 200 to 260 °C at a heating rate of 5 °C/min under a nitrogen atmosphere.

Table 1 Elemental compositions of three types of solders

Solder types	Sn (%)	Cu (%)	Ag (%)
Sn0.7Cu	99.3	0.7	–
Sn0.7Cu0.3Ag[a]	99.0	0.7	0.3
Sn0.7Cu + 0.3Ag[b]	99.0	0.7	0.3

[a] Prepared by alloying pure Sn, Cu and Ag metals

[b] Prepared by doping Ag nanoparticles into Sn0.7Cu solder paste

Solder/pad joints were fabricated to study the mechanical properties and microstructure, by reflowing solder balls on Cu pads (Diameter of 220 μm) metalized with Au/Ni layers. Then, solder joints were isothermally stored for up to 500 h in an oven with a temperature of 90 °C (363 K). The shear strength was studied by a ball shear tester (Dage series 4000) with a pendulum weight of 5.0 kg, at a shear speed of 500 μm/s. The average shear strength was calculated from the average value of fifteen test results, with the maximum and the minimum removed. Microhardness was investigated using a Vickers hardness tester (MXT-CXT, MATSUZAWA), with an applied load of 200 gf for 12 s. The average hardness was calculated from the average value of 15 test results, with the maximum and the minimum removed. To observe the microstructure, especially that of the IMC layer at the solder/pad interface, the solder joints were mounted in epoxy resin and then cross-sectioned, ground, polished and etched to make specimens. Before observation using scanning electron microscopy (SEM) in backscattered-electron (BSE) mode and using energy dispersive X-ray detection (EDX), the samples were dried and coated with a thin layer of Au. The thickness of the IMC layer was determined as the quotient of the IMC area, divided by the interface length—with the help of the professional image software, ImageJ.

In order to study the electromigration (EM) behavior, a current stressing model was built with the structure illustrated in Fig. 1. Solder balls were firstly reflowed onto a dummy chip, followed by a second reflow process to establish interconnections between the dummy chip and the substrate, which was aligned by using a flip-chip bonder

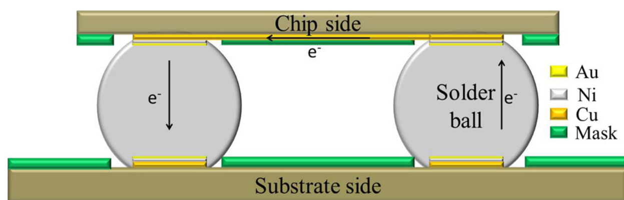

Fig. 1 Schematic illustration of the structure of EM test model

(Karl Suss 9493 Mauren). Test models were placed in an isothermal oven, at a temperature of 100 °C (373 K) and a current of 3 A was applied (giving an average current density of 0.79 × 10^4 A/cm^2). After stressing for 200, 400, and 600 h respectively, test models were taken out to make specimens. The microstructure at the cathodes and the anodes was studied using SEM and EDX.

The experimental and analysis processes of this work are summarized in Fig. 2.

3 Results

3.1 DSC test

Figure 3 showed the heat flow of three kinds of solders during DSC test. It was found that the liquidus temperature of Sn0.7Cu was 228.87 °C, which was somewhat higher than those of Sn0.7Cu0.3Ag (227.68 °C) and Sn0.7Cu + 0.3Ag (226.89 °C). The introduction of a small amount of Ag caused little change to the melting point, which has also been reported by other researchers [6, 9, 10]. Since the melting temperature does not change much, the same reflow profile can be used for all three solder pastes. In addition, similar sub-peaks were observed in the DSC curves of both Ag-

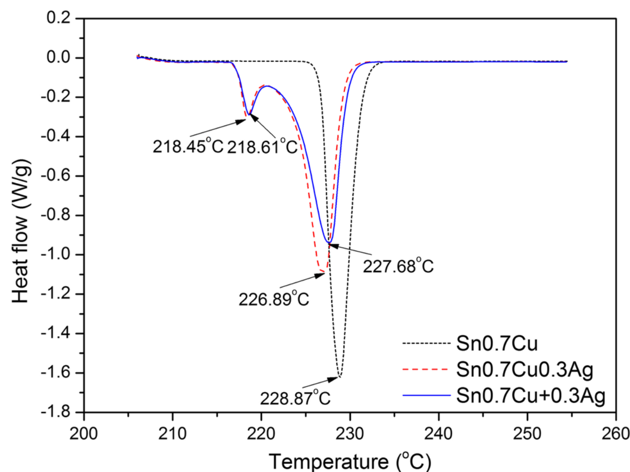

Fig. 3 DSC curves of three kinds of solders

incorporated solders, which could be ascribed to the changed crystal type and structure due to the introduction of Ag.

3.2 Microstructure evolution after thermal aging

SEM was used to study the microstructure morphology and composition. After the initial reflow, a scalloped IMC layer was formed at the solder/pad interface, as depicted in Fig. 4a. The composition of the IMC layer was identified to be 4.45 at% Au (the coating layer), 44.77 at% Sn, 26.60 at% Ni and 24.17 at% Cu from the EDX spectrum taken at spot P in Fig. 4a. By removing the Au, which mainly comes from the coating process, the IMC composition can be expressed as 46.86 at% Sn, 27.85 at% Ni and 25.29 at% Cu. As the composition did not correspond to any known IMC composition, it should be represented as a ternary Sn–Ni–Cu phase.

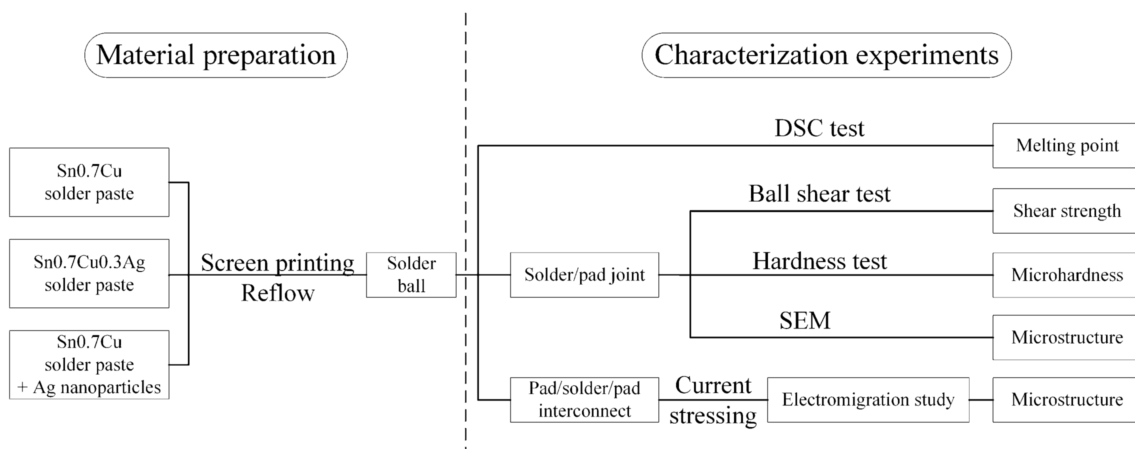

Fig. 2 Flowchart of experimental and analysis processes

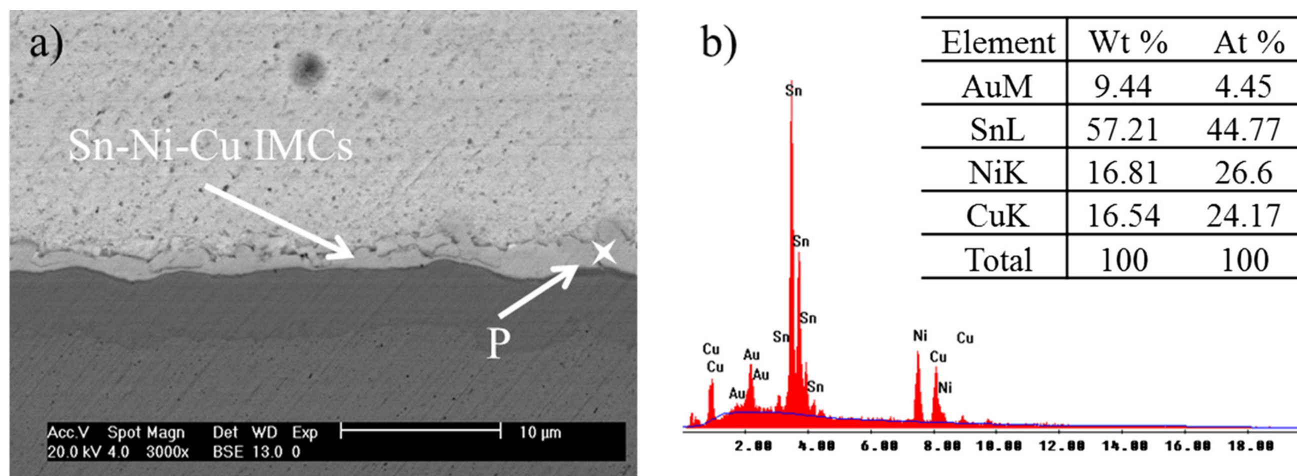

Element	Wt %	At %
AuM	9.44	4.45
SnL	57.21	44.77
NiK	16.81	26.6
CuK	16.54	24.17
Total	100	100

Fig. 4 **a** SEM image of interfacial IMCs layer of Sn0.7Cu solder, **b** EDX spectrum taken at spot P

After isothermal aging, the samples were cross-sectioned, in order to observe the evolution of the microstructure inside the solder joints. SEM images of interfacial IMC layers labeled with solder type and aging time are listed in Fig. 5, in which SC, SCA, and SC + A stand for Sn0.7Cu, Sn0.7Cu0.3Ag and Sn0.7Cu + 0.3Ag, respectively. The scalloped Sn–Ni–Cu IMC became smooth at the top surface—and grew thicker, after aging for 500 h. The thickness of the interfacial Sn–Ni–Cu IMC layer was measured using ImageJ and is plotted using OriginLab in Fig. 6. The average IMC layer thickness of the as-reflowed solders was 1.04 μm for Sn0.7Cu, 1.06 μm for Sn0.7Cu0.3Ag and 0.92 μm for Sn0.7Cu + 0.3Ag. As the thermal aging continued, the IMC layers grew thicker for all three solders. On average, Sn0.7Cu was found to have the thickest IMC layer, while Sn0.7Cu + 0.3Ag had the thinnest IMC layer. The

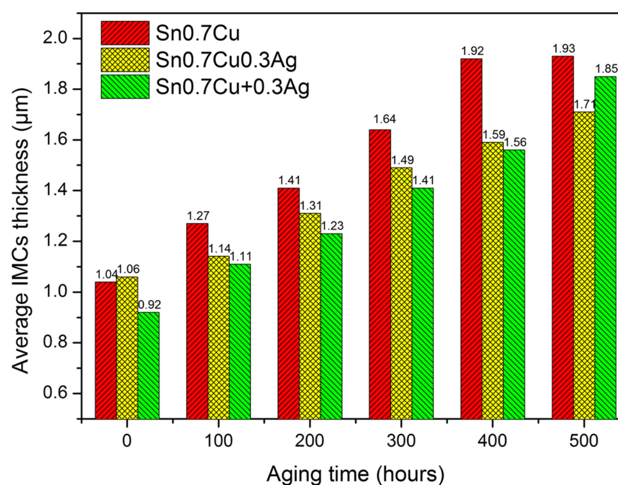

Fig. 6 Average IMC layer thicknesses subjected to different aging time

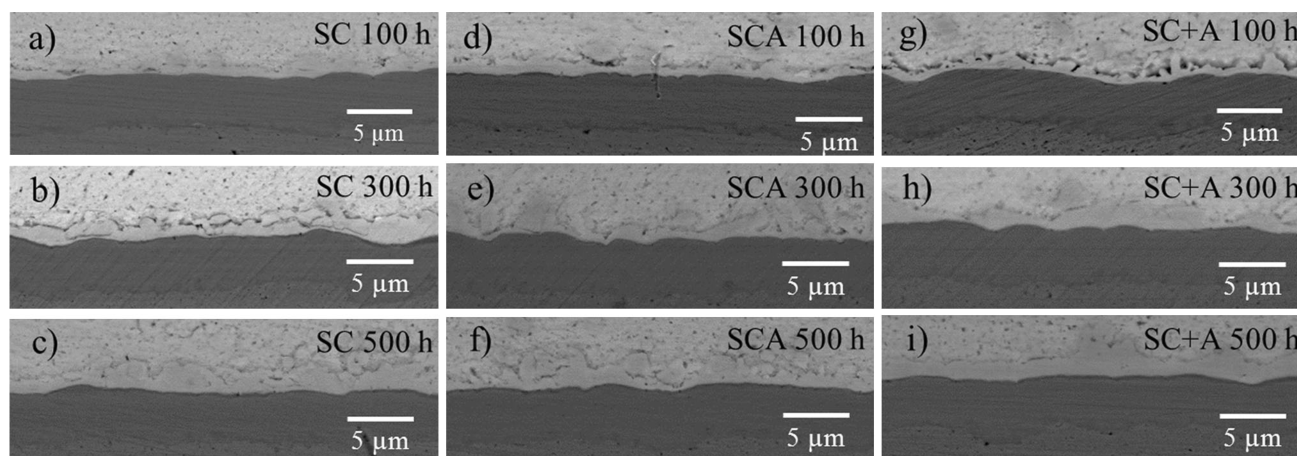

Fig. 5 SEM images of interfacial IMCs layers with solder type and aging time labeled, **a–c** Sn0.7Cu, **d–f** Sn0.7Cu0.3Ag, and **g–i** Sn0.7Cu + 0.3Ag

measured results revealed that Ag addition significantly inhibited the interfacial IMC layer growth, with an average rate of decrease of 8.86 % in Sn0.7Cu0.3Ag and 12.30 % in Sn0.7Cu + 0.3Ag.

3.3 Microstructure evolution after current stressing

After current stressing for various times, interconnects were cross-sectioned to observe the microstructure evolution at both the anodes and the cathodes. At the corners of Sn0.7Cu anodes, as seen in Fig. 7a–c, some IMCs have piled up. This phenomenon was due to the polarity effect of current stressing [19]. Metal atoms were driven to migrate along the direction of electron flow after momentum transfer produced by collisions with the electrons. Sn, Ag, and Cu atoms were found to have different migration speeds, due to their different atomic weights and effective charge numbers, which results in phase segregation in the solder matrix [16, 20]. As shown in Fig. 7, Cu was found to accumulate at the anode and form a thicker Sn–Ni–Cu IMC layer after reacting with surrounding Ni and Sn. Considering that Ni and Sn were sufficient, Cu atoms could be viewed as a controller of the Sn–Ni–Cu IMC region growth. EDX results showed that, at the IMC/solder interface, the Cu concentration was as high as 41.73 at%—while, at the pad/IMC interface, it was 19.27 at% in Fig. 7c. This high Cu concentration at IMC/solder interface justifies our contention that a large number of Cu atoms are transported from the bulk solder to the anode interface. In Fig. 7i, large amounts of Cu-rich phases were observed in the vicinity of the anode interface, since they had not yet reached the Sn0.7Cu + 0.3Ag anode.

The thicknesses of the anode IMC layers are plotted in Fig. 8 as a function of the stressing time. It was found that the anode IMC layers in all three types of solders became thicker as the

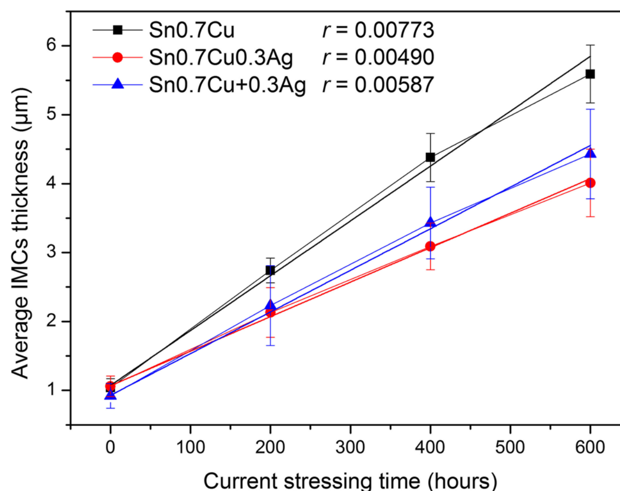

Fig. 8 Average thickness of anode IMCs layer subjected to stressing time at a temperature of 373 K and a current density of 0.79×10^4 A/cm^2

stressing time increased. Before current stressing, the IMC layer thicknesses of the three solders were 1.04, 1.06 and 0.92 μm—for Sn0.7Cu, Sn0.7Cu0.3Ag, and Sn0.7Cu + 0.3Ag, respectively. As current stressing continued, the IMC layers became thicker in an approximately linear relationship with stressing time. After 600 h of current stressing, the IMC layers grew to 5.59 μm (Sn0.7Cu), 4.01 μm (Sn0.7Cu0.3Ag), and 4.43 μm (Sn0.7Cu + 0.3Ag), respectively. Linear fitting was carried out in order to evaluate the growth rate of the IMC layer. The slope rate r for the three solders was calculated to be 0.00773 μm/h (2.15×10^{-10} cm/s) for Sn0.7Cu, 0.00490 μm/h (1.36×10^{-10} cm/s) for Sn0.7Cu0.3Ag, and 0.00587 μm/h (1.63×10^{-10} cm/s) for Sn0.7Cu + 0.3Ag. With the addition of elemental Ag, the growth rate of the Sn–Ni–Cu IMC layer decreased in both the Sn0.7Cu0.3Ag and the Sn0.7Cu + 0.3Ag solders. Furthermore, Sn0.7Cu0.3Ag was found to be more

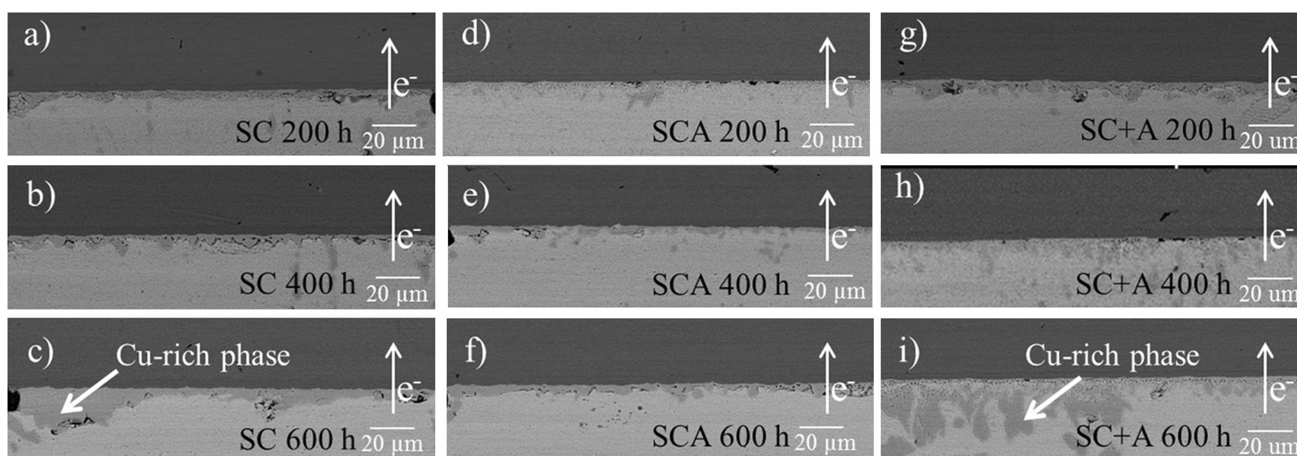

Fig. 7 SEM images of IMCs layers at the anodes with solder type and stressing time labeled, **a–c** Sn0.7Cu, **d–f** Sn0.7Cu0.3Ag, and **g–i** Sn0.7Cu + 0.3Ag. The direction of electron flow is indicated by the *vertical arrows*

effective in suppressing the IMC layer growth than Sn0.7Cu + 0.3Ag, as will be discussed later.

Figure 9 illustrates Sn–Ni–Cu IMC regions formed at the cathodes of three solders after current stressing for up to 600 h. As compared with the anodes, the cathodes have thinner Sn–Ni–Cu IMCs layers with rough surfaces, which were in wicker shapes and grew into the solder matrix. The thickness of the IMC layers formed at the cathodes was a balance between IMC dissolution due to EM—and IMC growth due to thermal aging. As the thickness of the cathode IMC layers was hard to determine, only the anode IMCs layers were studied systematically.

3.4 Mechanical properties

The shear strength is one of the most important mechanical properties related to the reliability of solder joints [2]. As solder joints may accumulate residual stress during service, superior shear strength is a guarantee of the reliability of electronic products [21]. Figure 10 lists the shear strengths of three solder joints subjected to various aging times. Sn0.7Cu0.3Ag solder was found to have the highest shear strength in all three solder joints regardless of aging time. The average shear strength of as-reflowed Sn0.7Cu0.3Ag solder joints was 3.24 N, which was 26.25 % higher than for Sn0.7Cu solder (2.57 N) and 12.79 % higher than for the composite Sn0.7Cu + 0.3Ag solder (2.87 N). As aging continued, all three solder joints showed a decrease in shear strength. After aging for 200 h, the shear strength of Sn0.7Cu + 0.3Ag solder joints decreased to the same level as Sn0.7Cu. After aging for 500 h, the average shear strength of Sn0.7Cu0.3Ag solder joints decreased to 2.14 N, which was 33.98 % lower than for the as-reflowed Sn0.7Cu0.3Ag solder joints (3.24 N). For Sn0.7Cu and Sn0.7Cu + 0.3Ag solder joints, the average shear strength decreased to 1.87 N and 1.97 N, after 500 h of aging, respectively. As a result, Ag addition into Sn0.7Cu by both alloying and doping methods was confirmed to reinforce the shear strength of Sn0.7Cu solder. Moreover, the alloyed Sn0.7Cu0.3Ag was superior in the enhancement and maintenance of higher shear strength than the doped Sn0. 7Cu + 0.3Ag.

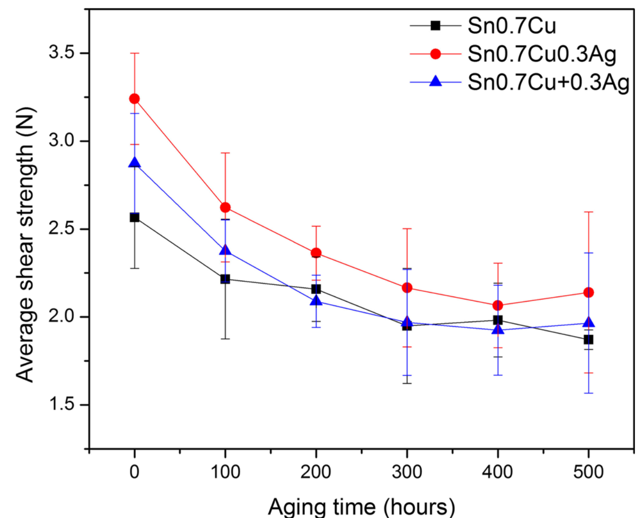

Fig. 10 Average shear strength of solder joints as a function of aging time, at a temperature of 363 K

Hardness characterizes the durability and suitability of solders during working [22]. Figure 11 illustrates the microhardness of three types of solder joint after aging for 0, 300 and 500 h. The average microhardness for as-reflowed solder joints was 9.6 Hv for Sn0.7Cu, 9.9 Hv for Sn0.7Cu + 0.3Ag, and 10.0 Hv for Sn0.7Cu0.3Ag, respectively. As the aging time increased, the solder joints deteriorated in hardness, with a rate of decrease of 4.17 % for Sn0.7Cu, 2.00 % for Sn0.7Cu0.3Ag, and 2.02 % for

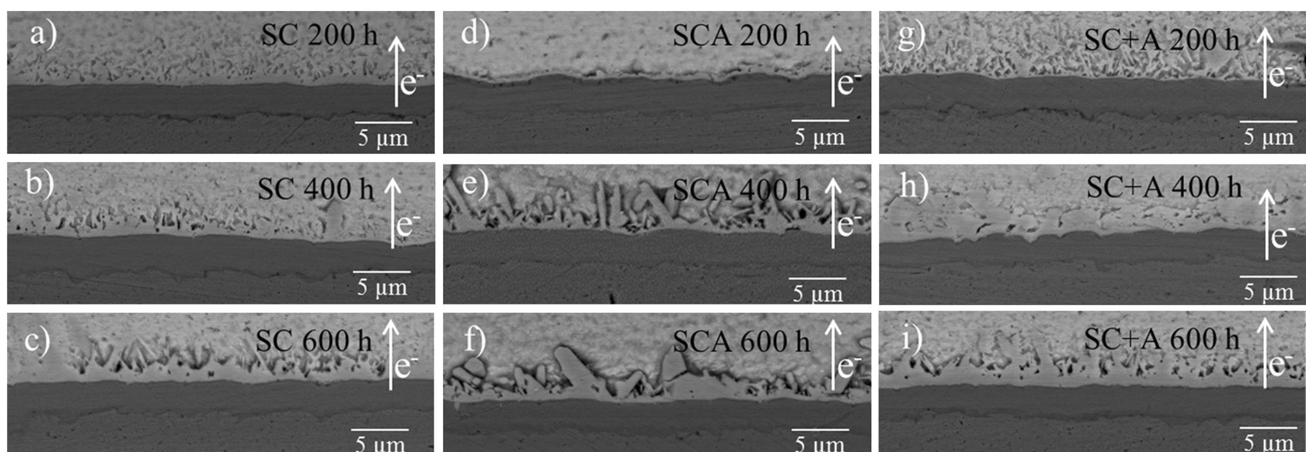

Fig. 9 SEM images of IMCs layers at the cathodes with solder type and stressing time labeled, **a–c** Sn0.7Cu, **d–f** Sn0.7Cu0.3Ag, and **g–i** Sn0.7Cu + 0.3Ag

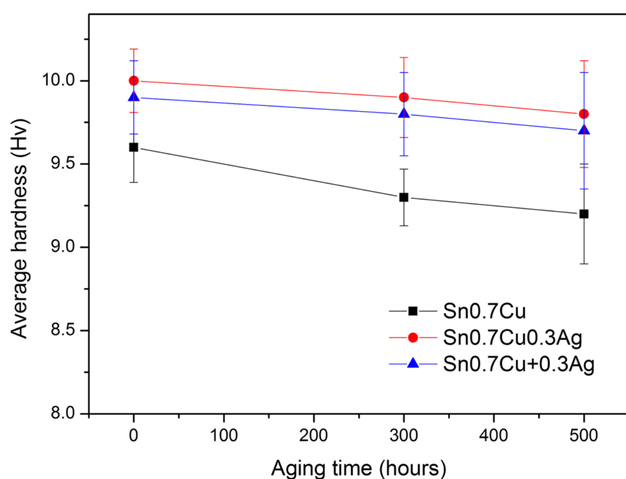

Fig. 11 Average microhardness of solder joints as a function of aging time, at a temperature of 363 K

Sn0.7Cu + 0.3Ag, after 500 h aging. The hardness of Ag-incorporated solders was found to be higher than that of plain Sn0.7Cu solder, while Sn0.7Cu0.3Ag maintained the highest hardness, regardless of aging time. Yi et al. [14] have also reported hardness reinforcement in Ag-modified Sn58Bi solder, which can be ascribed to the formation of dispersed Ag_3Sn IMCs in the solder matrix. The differences between the Sn0.7Cu0.3Ag and Sn0.7Cu + 0.3Ag were due to the differences in the shape and distribution of Ag_3Sn IMCs. Further analysis will be discussed in a later section.

4 Discussion

Our experimental results have demonstrated that the introduction of the element Ag into Sn0.7Cu solder paste leads to reinforced mechanical strength and higher resistance to EM. Several mechanisms can be used to explain the improvements.

Zener's relationship gives the relationship between the second-phase particle-size and the grain-size, as expressed below [23]:

$$R = \frac{4r}{3\zeta} \quad (1)$$

where R is the average dimension of grains, r is the average diameter of particles and ζ is the volume fraction of particles. According to Eq. 1, small-sized (r) particles cause a finer microstructure (R) in the bulk solder.

According to the Hall–Petch strengthening mechanism, the mechanical strength is strongly affected by grain size [24]:

$$\sigma_{Hall-Petch} = \sigma_0 + K_y d^{-1/2} \quad (2)$$

where $\sigma_{Hall-Petch}$ is the yield stress, σ_0 and K_y are material constants - and d is the average grain diameter. There are more grain boundaries in materials with finer microstructure, which require more energy for dislocations to alter direction. According to Eq. 2, a finer microstructure (d) results in a higher yield stress (σ), which means reinforcement in the mechanical strength.

The incorporation of nano-particles may enhance the mechanical strength of the solder joints by obstructing dislocation motions. This relation is described by the Orowan mechanism, as expressed by the equation below [25]:

$$\sigma_{Org} = \frac{2Gb}{\lambda} \quad (3)$$

where σ_{Org} is the yield stress, G is the shear modulus of the material matrix, b is the Burger's vector of the dislocation and λ is the distance between dispersed particles. Dislocations will bow to form Orowan loops around the particles, which results in the end of dislocation movement. According to Eq. 3, the yield stress of solder joints will be larger if the nano-particles in the bulk solder are distributed compactly.

From Eq. 1–3, it can be concluded that the mechanical strength of Ag incorporated solders was enhanced by the introduction of the dispersed Ag_3Sn particles, which refined the microstructure - and acted as a second phase in the solder matrix to stop dislocation motion. In the research of Seok-Hwan Huh [26], microstructure observation revealed that 0.3 wt % of Ag addition into Sn0.7Cu solder reduced remarkably the grain size of Sn in the bulk solder. This reduction in Sn grain size due to Ag addition was also reported by A.A. El-Daly [27]. Furthermore, the smaller size and more compact distribution of the second-phase particles results in a greater improvement in the mechanical strength.

Figure 12 shows two images of bulk solder with dispersed Ag_3Sn particles, a) Sn0.7Cu0.3Ag and b) Sn0.7Cu + 0.3Ag. The average size of the Ag_3Sn particles was measured using ImageJ. The small dot-like Ag_3Sn particles in the Sn0.7Cu0.3Ag solder were measured to have an average diameter of 0.3219 μm (corresponding to an area of 0.0814 μm^2), while the rod shaped Ag_3Sn particles in the Sn0.7Cu + 0.3Ag solder had an average diameter of 1.1474 μm (corresponding to an area of 1.0339 μm^2). The measured results justified the conclusion that the superior mechanical strength of the Sn0.7Cu0.3Ag solder was due to the smaller sized and wider distributed Ag_3Sn particles. The molar volumes of Ag, Sn, and Ag_3Sn were 1.12×10^{-5}, 2.09×10^{-5}, and 4.53×10^{-5} $m^3 mol^{-1}$, respectively [28]. Assuming that an Ag nanoparticle with an average diameter of 70 nm reacts completely with Sn, it will produce an Ag_3Sn particle with an average diameter of $70 \times \sqrt[3]{45.3/(11.2 \times 3)} = 77$ nm, which is much smaller than 1.1474 μm (1147.4 nm) we

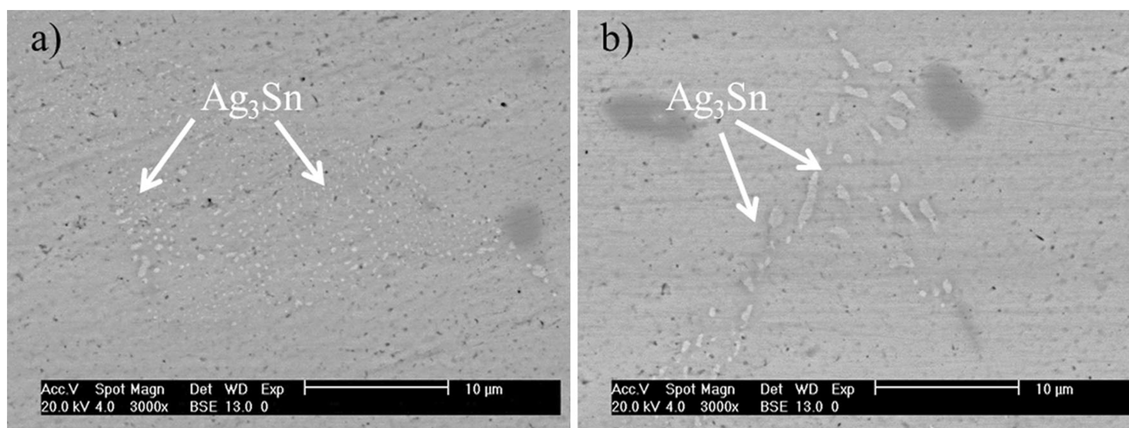

Fig. 12 SEM images of Ag_3Sn particles in solder matrix, **a** Sn0.7Cu0.3Ag, **b** Sn0. 7Cu + 0.3Ag

measured in Sn0.7Cu + 0.3Ag. This difference in Ag_3Sn particle size between theoretical calculation and experimental measurement was due to the agglomeration of Ag and Ag_3Sn nanoparticles during reflow soldering [14]. As nanoparticles are highly surface-active, Ag and Ag_3Sn nanoparticles will agglomerate and form large particles, in order to reduce the surface energy and achieve stability [6]. Furthermore, surface-active Ag_3Sn particles will be adsorbed into the interfacial IMC layer [14], which may inhibit the IMC layer growth. Figure 13 shows: a) an SEM image of the interfacial IMC layer in an Sn0.7Cu + 0.3Ag solder joint after thermal aging for 500 h, - and b) an EDX spectrum taken at spot Q. The EDX results confirmed that the bright phase adsorbed at the top surface of the interfacial IMCs layer was Ag_3Sn. These particles cut off the continuous formation of the IMC layer - and hindered the diffusion of Cu atoms to inhibit the IMC layer growth.

It was noteworthy that, in the thermal aging case, Sn0.7Cu + 0.3Ag had a thinner IMC layer than Sn0.7Cu0.3Ag - while, in the current stressing case, Sn0.7Cu0.3Ag was found to have a thinner IMC layer than Sn0.7Cu + 0.3Ag. In the thermal aging case, the adsorbed Ag_3Sn particles in Sn0.7Cu + 0.3Ag destroyed the continuity of the IMC layer and retarded the formation of the IMC layer, by obstructing the diffusion of the Cu atoms from the Cu pad. As a result, the IMC layer in Sn0.7Cu + 0.3Ag was thinner than in Sn0.7Cu0.3Ag under thermal aging. However, in the current stressing case, Cu atoms in the Cu-rich phase mainly came from bulk solder. This meant that the accumulation rate of Cu atoms was mainly affected by the dispersed Ag_3Sn particles in the solder matrix. The smaller size and wider distribution of Ag_3Sn particles in Sn0.7Cu0.3Ag contributed to more effective suppression of Cu atoms migration as more obstacles existed. As a result, the Cu-rich phase at the anodes was thinner in Sn0.7Cu0.3Ag than in Sn0.7Cu + 0.3Ag, under current stressing.

The Sn-Ni-Cu IMC layer at both the anodes and the cathodes thickened when a current was applied. In this work, only the anode IMCs layers are discussed systematically to evaluate the performance of the solders under

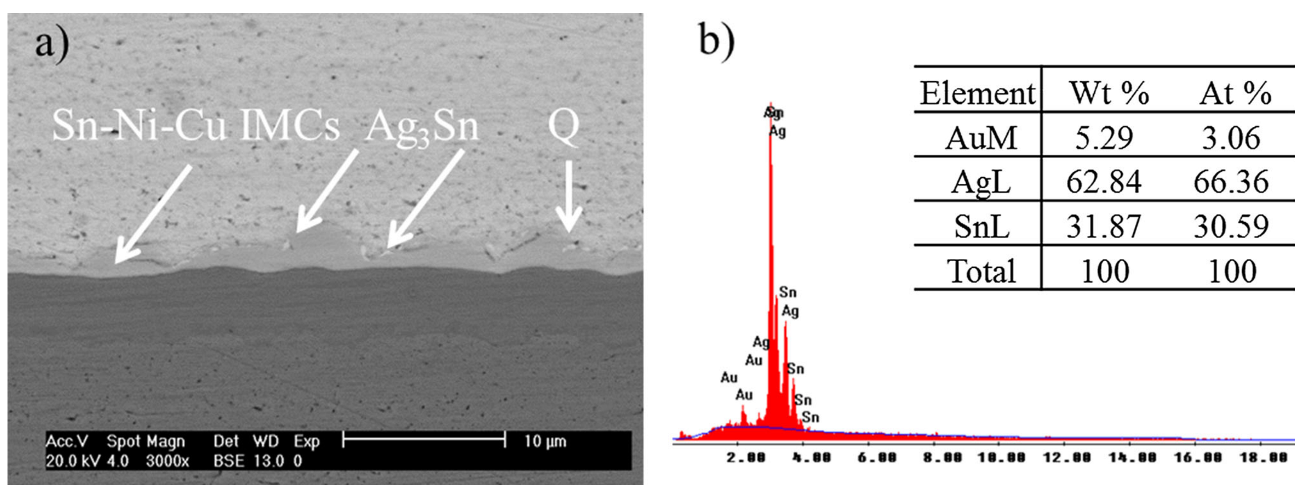

Element	Wt %	At %
AuM	5.29	3.06
AgL	62.84	66.36
SnL	31.87	30.59
Total	100	100

Fig. 13 **a** SEM images of interfacial IMCs layer of Sn0.7Cu + 0.3Ag after 500 h aging, **b** EDX spectrum taken at spot Q

Table 2 DZ^* values of three types of solders

Solder types	r (cm/s)	J_{em} (atoms/cm^{2}s)	DZ^* (cm^2/s)
Sn0.7Cu	2.15×10^{-10}	5.31×10^{12}	3.49×10^{-9}
Sn0.7Cu0.3Ag	1.36×10^{-10}	3.36×10^{12}	1.91×10^{-9}
Sn0.7Cu + 0.3Ag	1.63×10^{-10}	4.02×10^{12}	2.64×10^{-9}

EM testing. According to L.L. Chen, the atomic flux of Cu due to EM can be described by [29]:

$$J_{em} = rd\frac{N}{m}w \quad (4)$$

where r is the accumulation rate of Cu (listed in Table 2), d is the density of Cu (8.92 g/cm^3), N is Avogadro's number (6.02×10^{23} atoms/mol), and m is the atomic weight of Cu (63.55 g/mol), w is the concentration of Cu due to EM.

The accumulation rate (r) of Cu can be expressed by the IMC thickness growth rate, i.e., the slopes in Fig. 8. The pre-existed Cu concentration in the vicinity of anode IMCs layer was calculated to be 1.28 at % (0.7 wt %) according to the method of Chen [29]. Due to current stressing, the average Cu concentration in the Cu-rich phase increased to 30.50 at %, which was calculated from the average value of the Cu concentrations at the two ends of the anode IMC layer. So the increased Cu concentration w due to EM can be calculated as 30.50-1.28 at % = 29.22 at %. By inserting the values of the parameters into Eq. 4, the value of J_{em} for the three different solders can be obtained (listed in Table 2). According to the theory of K.N. Tu, the atomic flux of Cu due to EM can also be described by the following equation [30]:

$$J_{em} = C\frac{D}{kT}Z^* e\rho j \quad (5)$$

where C is the concentration (4.77×10^{20} atoms/cm^3 for Sn0.7Cu, 4.78×10^{20} atoms/cm^3 for Sn0.7Cu0.3Ag and Sn0.7Cu + 0.3Ag, according to the method proposed by L.L. Chen [29]), D is the diffusion coefficient, k is the Boltzmann constant (1.38×10^{-23} J/K), T is the absolute temperature (373 K), Z^* is the effective charge number, e is the electronic charge (1.6×10^{-19} C), ρ is the resistivity (0.13 μΩ·m for Sn0.7Cu, 0.15 μΩ·m for Sn0.7Cu0.3Ag, according to the Amtech datasheet), and j is the current density (0.79×10^4 A/cm^2).

The product of diffusivity D and effective charge number Z^* is a measure of the EM rate, which can be expressed by changing the form of Eq. 5):

$$DZ^* = \frac{J_{em}kT}{e\rho j}. \quad (6)$$

Calculation showed that the value of DZ^* was lowered from 3.49×10^{-9} cm^2/s for Sn0.7Cu to 1.91×10^{-9} cm^2/s for Sn0.7Cu0.3Ag and 2.64×10^{-9} cm^2/s for Sn0.7Cu + 0.3Ag. We can conclude that the introduction of Ag inhibited the migration of Cu atoms in both Sn0.7Cu0.3Ag and Sn0.7Cu + 0.3Ag. Moreover, the alloying method was found to be more effective in preventing the migration of the atoms, as the DZ^* value for Sn0.7Cu0.3Ag was 27.65 % lower than that for Sn0.7Cu + 0.3Ag.

5 Conclusions

The microstructure and mechanical strength of pristine and Ag-modified Sn0.7Cu solders were thoroughly studied in this work. DSC curves showed that the addition of a small amount of Ag slightly affects the liquidus temperature, as the melting points of the three solders were 228.87 °C (Sn0.7Cu), 227.68 °C (Sn0.7Cu0.3Ag), and 226.89 °C (Sn0.7Cu + 0.3Ag), respectively. It was found that the addition of Ag into Sn0.7Cu solder improves the mechanical strength for both methods of addition. The shear strength of Sn0.7Cu was reinforced by 26.25 % in the Sn0.7Cu0.3 solder joints (fabricated by the alloying method) and 12.79 % in the Sn0.7Cu + 0.3Ag solder joints (fabricated by the doping method). The microhardness of Sn0.7Cu was also enhanced by 4.17 % and 3.13 % in Sn0.7Cu0.3Ag and Sn0.7Cu + 0.3Ag, respectively. The resistance to EM was also enhanced in Ag incorporated solders, as the product of diffusivity and effective charge number DZ^* was lowered from 3.49×10^{-9} cm/s (for Sn0.7Cu) to 1.91×10^{-9} cm/s (for Sn0.7Cu0.3Ag) and 2.64×10^{-9} cm/s (for Sn0.7Cu + 0.3Ag). These experimental results justified the conclusion that Sn0.7Cu0.3Ag has a better performance than Sn0.7Cu + 0.3Ag, which results from the smaller sized and more widely distributed Ag_3Sn particles in Sn0.7Cu0.3Ag. The poor improvement for Sn0.7Cu + 0.3Ag was due to the agglomeration and adsorption of Ag and Ag_3Sn particles. As a result, for the same concentration, the alloying method provides a greater enhancement over the plain Sn0.7Cu solder than the doping method, in both microstructure evolution and mechanical strength.

Acknowledgments The authors would like to acknowledge the financial support provided by the National Natural Science Foundation of China/Research Grants Council of Hong Kong (NSFC/RGC), Ref. No. 9054008 (Electromigration and Thermomigration Studies in Nanostructured Composite Electronic Interconnects for Nanoelectronics Applications), and the Research Grants Council of Hong Kong, Ref. No. 9041636 (A Study of Nanostructured Electronic Interconnects-preparation, Characterization and Integration). The authors would also like to thank Dr. Yi Li for providing experiment guidance. Also, thanks to Professor Richard De La Rue, University of Glasgow, Scotland, U.K., for critical review of the paper.

References

1. K. Tu, A. Gusak, M. Li, Physics and materials challenges for lead-free solders. J. Appl. Phys. **93**, 1335–1353 (2003)
2. H. Ma, J.C. Suhling, A review of mechanical properties of lead-free solders for electronic packaging. J. Mater. Sci. **44**, 1141–1158 (2009)
3. R. Chinnam, C. Fauteux, J. Neuenschwander, J. Janczak-Rusch, Evolution of the microstructure of Sn–Ag–Cu solder joints exposed to ultrasonic waves during solidification. Acta Mater. **59**, 1474–1481 (2011)
4. http://www.infomine.com/investment/metal-prices/. Accessed 16 Sep 2015
5. X. Chen, A. Hu, M. Li, D. Mao, Study on the properties of Sn–9Zn–xCr lead-free solder. J. Alloys Compd. **460**, 478–484 (2008)
6. H. Sun, Q. Li, Y. Chan, A study of Ag additive methods by comparing mechanical properties between Sn57. 6Bi0.4Ag and 0.4 wt% nano-Ag-doped Sn58Bi BGA solder joints. J. Mater. Sci. Mater. Electron. **25**, 4380–4390 (2014)
7. S. Hwang, J. Lee, Z. Lee, Microstructure of a lead-free composite solder produced by an in situ process. J. Electron. Mater. **31**, 1304–1308 (2002)
8. C. Wu, D. Yu, C. Law, L. Wang, Properties of lead-free solder alloys with rare earth element additions. Mater. Sci. Eng. R Rep. **44**, 1–44 (2004)
9. M. Amagai, A study of nanoparticles in Sn–Ag based lead free solders. Microelectron. Reliab. **48**, 1–16 (2008)
10. L. Tsao, M. Wu, S. Chang, Effect of TiO_2 nanoparticles on the microstructure and bonding strengths of Sn0. 7Cu composite solder BGA packages with immersion Sn surface finish. J. Mater. Sci. Mater. Electron. **23**, 681–687 (2012)
11. C. Zou, Y. Gao, B. Yang, Q. Zhai, Melting and solidification properties of the nanoparticles of Sn3.0Ag0.5Cu lead-free solder alloy. Mater. Charact. **61**, 474–480 (2010)
12. K. Bukat, M. Koscielski, J. Sitek, M. Jakubowska, A. Mlozniak, Silver nanoparticles effect on the wettability of Sn–Ag–Cu solder pastes and solder joints microstructure on copper. Solder. Surf. Mount Technol. **23**, 150–160 (2011)
13. A. Nadia, A. Haseeb, Understanding the effects of addition of copper nanoparticles to Sn-3.5 Ag solder. Sold. Surf. Mount Technol. **23**, 68–74 (2011)
14. Y. Li, Y. Chan, Effect of silver (Ag) nanoparticle size on the microstructure and mechanical properties of Sn58Bi-Ag composite solders. J. Alloys Compd. **645**, 566–576 (2015)
15. M.N. Bashir, A. Haseeb, A.Z. Rahman, M.A. Fazal, C. Kao, Reduction of electromigration damage in SAC305 solder joints by adding Ni nanoparticles through flux doping. J. Mater. Sci. **50**, 6748–6756 (2015)
16. S. Xu, Y.C. Chan, K. Zhang, K. Yung, Interfacial intermetallic growth and mechanical properties of carbon nanotubes reinforced Sn3.5Ag0.5Cu solder joint under current stressing. J. Alloys Compd. **595**, 92–102 (2014)
17. T. Chuang, M. Wu, S. Chang, S. Ping, L. Tsao, Strengthening mechanism of nano-Al_2O_3 particles reinforced Sn3.5Ag0.5Cu lead-free solder. J. Mater. Sci. Mater. Electron. **22**, 1021–1027 (2011)
18. A.K. Gain, T. Fouzder, Y.C. Chan, A. Sharif, N.B. Wong, W.K. Yung, The influence of addition of Al nano-particles on the microstructure and shear strength of eutectic Sn–Ag–Cu solder on Au/Ni metallized Cu pads. J. Alloys Compd. **506**, 216–223 (2010)
19. H. Gan, K. Tu, Polarity effect of electromigration on kinetics of intermetallic compound formation in Pb-free solder V-groove samples. J. Appl. Phys. **97**, 063514 (2005)
20. Y.C. Chan, D. Yang, Failure mechanisms of solder interconnects under current stressing in advanced electronic packages. Prog. Mater Sci. **55**, 428–475 (2010)
21. X. Hu, Y. Chan, K. Zhang, K. Yung, Effect of graphene doping on microstructural and mechanical properties of Sn–8Zn–3Bi solder joints together with electromigration analysis. J. Alloys Compd. **580**, 162–171 (2013)
22. A.K. Gain, T. Fouzder, Y.C. Chan, W.K. Yung, Microstructure, kinetic analysis and hardness of Sn–Ag–Cu–1wt% nano-ZrO_2 composite solder on OSP-Cu pads. J. Alloys Compd. **509**, 3319–3325 (2011)
23. R. Abbaschian, R. Reed-Hill, *Physical Metallurgy Principles* (Cengage Learning, Stanford, 2008), pp. 255–256
24. W.D. Callister, *Fundamentals of Materials Science and Engineering: an Interactive e-Text* (Wiley, New York, 2012), p. 189
25. J.W. Martin, *Micromechanisms in particle-hardened alloys* (Cambridge UP, New York, 1980), pp. 60–62
26. S. Huh, K. Kim, K. Suganuma, Effects of Ag addition on the microstructural and mechanical properties of Sn–Cu eutectic solder. Mater. Trans. **42**, 739–744 (2001)
27. A. El-Daly, A. Hammad, Enhancement of creep resistance and thermal behavior of eutectic Sn–Cu lead-free solder alloy by Ag and in-additions. Mater. Des. **40**, 292–298 (2012)
28. K. Sim, J. Lee, Phase stability of Ag–Sn alloy nanoparticles. J. Alloys Compd. **590**, 140–146 (2014)
29. L. Chen, C. Chen, Electromigration study in the eutectic SnBi solder joint on the Ni/Au metallization. J. Mater. Res. **21**, 962–969 (2006)
30. K. Tu, Electromigration in stressed thin films. Phys. Rev. B **45**, 1409 (1992)